

# Linear and Nonlinear Optical Spectroscopy at the Nanoscale with Photoinduced Force Microscopy

Junghoon Jahng,<sup>†</sup> Dmitry A. Fishman,<sup>‡</sup> Sung Park,<sup>||</sup> Derek B. Nowak,<sup>||</sup> Will A. Morrison,<sup>||</sup> H. Kumar Wickramasinghe,<sup>§</sup> and Eric O. Potma\*,<sup>‡</sup>

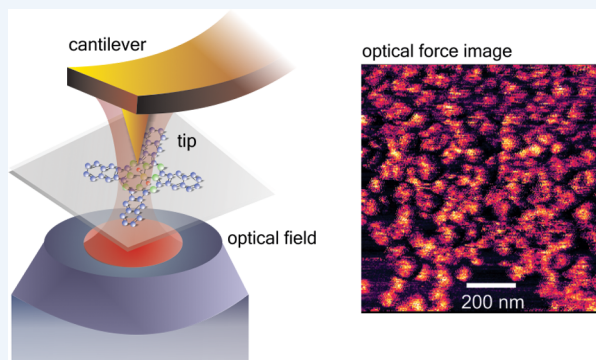
<sup>†</sup>Department of Physics and Astronomy, <sup>‡</sup>Department of Chemistry, and <sup>§</sup>Department of Electrical Engineering and Computer Sciences, University of California, Irvine, California 92697, United States

<sup>||</sup>Molecular Vista Inc., 6840 Via Del Oro, San Jose, California 95119, United States

**CONSPECTUS:** The enormous advances made in nanotechnology have also intensified the need for tools that can characterize newly synthesized nanostructures with high sensitivity and with high spatial resolution. Many existing tools with nanoscopic resolution or better, including scanning electron microscopy (SEM), atomic force microscopy (AFM), and scanning tunneling microscopy (STM) methods, can generate highly detailed maps of nanoscopic structures. However, while these approaches provide great views of the morphological properties of nanomaterials, it has proven more challenging to derive chemical information from the corresponding images. To address this issue, attempts have been made to dress existing nanoscopy methods with spectroscopic sensitivity. A powerful approach in this direction is the combination of scan probe techniques with optical illumination, which aims to marry the nanoscopic resolution provided by a sharp tip with the chemical selectivity provided by optical spectroscopy. Examples of this approach include existing techniques such as scattering-type scanning near-field optical microscopy and tip-enhanced Raman spectroscopy. A new and emerging technique in this direction is photoinduced force microscopy (PiFM), which enables spectroscopic probing of materials with a spatial resolution well under 10 nm.

In PiFM, the sample is optically excited and the response of the material is probed directly in the near-field by reading out the time-integrated force between the tip and the sample. Because the magnitude of the force is dependent on the photoinduced polarization in the sample, PiFM exhibits spectroscopic sensitivity. The photoinduced forces measured in PiFM are spatially confined on the nanometer scale, which translates into a very high spatial resolution even under ambient conditions. The PiFM approach is compatible with a wide range optical excitation frequencies, from the visible to the mid-infrared, enabling nanoscale imaging contrast based on either electronic or vibrational transitions in the sample. These properties make PiFM an attractive method for the visualization and spectroscopic characterization of a vast variety of nano materials, from semiconducting nanoparticles to polymer thin films to sensitive measurements of single molecules.

In this Account, we review the principles of the PiFM technique and discuss the basic components of the photoinduced force microscope. We highlight the imaging properties of the PiFM instrument and demonstrate the inherent spectroscopic sensitivity of the technique. Furthermore, we show that the PiFM approach can be used to probe both the linear and nonlinear optical properties of nano materials. In addition, we provide several examples of PiFM imaging applications.



## INTRODUCTION

Advances in the fabrication of nanoscale materials have led to vast diversity of nanostructures that span a wide range of chemical compositions and morphologies. The new nanoscale synthesis capabilities have also triggered a need for analytical tools that can suitably characterize these nanomaterials. Chemical selectivity and a high spatial resolution are among the probing capabilities that facilitate analysis at the nanoscale. Although many existing techniques feature either chemical selectivity or nanoscale spatial resolution, the combination of both is not trivial to achieve.

Optical spectroscopy is a powerful analytical tool that allows noncontact probing of ensembles of nanostructures. The

electronic and vibrational transitions in the material that are accessible through optical spectroscopy form useful fingerprints for identifying or characterizing the specimen. When carried out in an optical microscope, spectroscopic measurements can be performed with sub-micrometer spatial resolution, as dictated by the diffraction limit of light. Although single nanostructures can be examined when sparsely distributed on the substrate surface, standard far-field optical microscopy is unable to resolve the spatial properties of nanomaterials on the relevant spatial scale. Even recent super-resolution techniques,<sup>1</sup>

Received: July 10, 2015

Published: October 9, 2015

which are based on the specific photophysics of selected chromophores, cannot be universally applied to enable spectroscopy measurements with nanoscale resolution.

A more direct way to bring spectroscopic sensitivity to the nanoscale is the use of near-field optical techniques. By exciting and/or detecting the nanotargets in the near-field, material properties can be examined at subdiffraction limited spatial resolution. Most spectroscopic near-field methods achieve high spatial resolution by using a sharp tip, which transmits the information from the near-field through scattering radiation to a far-field photodetector.<sup>2</sup> Examples of near-field vibrational spectroscopy include tip-enhanced Raman scattering methods<sup>3–6</sup> and near-field infrared techniques,<sup>7–9</sup> which have been utilized to interrogate nanostructured materials with a resolution down to several tens of nanometers.

The resolution in scattering-based near-field methods is governed by the spatial dimensions of the confined fields at the tip antenna. For practical tip designs, it is not trivial to reduce the size of the local field below ~10 nm, unless different physical effects at the tip are leveraged to further confine the effective probing volume. This notion also opens up the possibility of exploring methods that use alternative mechanisms, beyond the detection of scattered radiation, for reading out the local response near the tip–sample junction.

One high-resolution, nonoptical detection strategy is based on registering the local force in the junction. Used extensively in atomic force microscopy (AFM) methods,<sup>10–12</sup> local forces, such as electrostatic, van der Waals, and Casimir forces, manifest themselves over nanometer scale distances between the tip and the sample, translating into a high lateral resolution that routinely dips well below 10 nm under optimized conditions. Under optical illumination of the tip–sample junction, photoinduced forces are present as well, which can be detected by modulating the incident light and employing demodulation detection techniques. Among the photoinduced forces, which can generally be divided into scattering and gradient forces, are attractive interactions between the optically driven tip dipole and the optically induced polarization of the sample material.<sup>13</sup> Such forces can be in the pN range, and can be conveniently detected with demodulation techniques. Since photoinduced forces carry information on the sample's optical polarizability, it is possible to use this quantity as a read-out mechanism for probing spectroscopic transitions with sub-10 nm spatial resolution.

The photoinduced force microscope (PiFM) combines the high spatial resolution of the AFM microscope with the analytical capabilities provided by optical spectroscopy. As shown by Wickramasinghe and co-workers in 2010, PiFM can generate high-resolution images with contrast based on linear absorption of light by chromophores in the sample.<sup>14</sup> In addition to linear spectroscopic contrast, PiFM has also been used to probe nonlinear optical transitions in materials, including nonlinear excited state absorption<sup>15</sup> and stimulated Raman vibrational transitions.<sup>16</sup> PiFM is different from other spectroscopically sensitive force-detection techniques, such as infrared-based AFM,<sup>17–20</sup> in that it can be conducted in noncontact mode, producing high-resolution measurements in the sub-10 nm range under ambient conditions.

PiFM is a new technique. The theoretical description of the PiFM approach is still under development, although early models appear already capable of extracting quantitative information from PiFM images.<sup>21,22</sup> Despite the young age of the PiFM technology, it is clear that the merger of AFM-like

imaging properties with spectroscopic sensitivity constitutes an important leap forward for the visualization and characterization of nanoscale materials. In this Account, we describe the basic principles of the PiFM technique, discuss the layout of the instrument, present the imaging properties of the technique and highlight nascent applications enabled by PiFM.

## ■ PRINCIPLES OF PIFM

PiFM measures the photoinduced forces between a sharp tip and the sample. A schematic of the interaction between the tip and the (nano)particle is given in Figure 1, where the system is

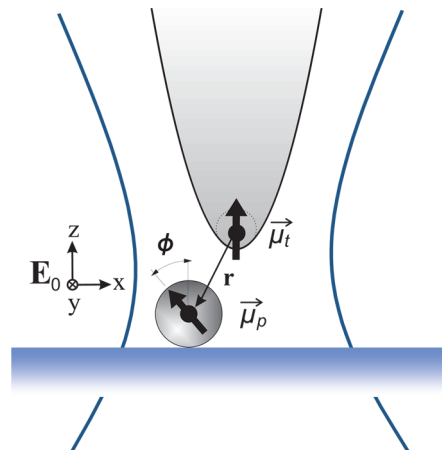


**Figure 1.** Schematic of the interaction between the photoinduced tip-dipole and the photoinduced dipole of the target particle in the focal plane of a tightly focused field. The focal field  $E_0$  results from a plane wave, which is linearly polarized in the  $x$ -direction, and is focused by a high numerical aperture lens onto the sample.

illuminated by an incoming light field  $E_0$ . The situation in the tip–sample junction can be described by approximating both the tip apex and the sample particle as polarizable spheres and considering only dipolar contributions. In this scenario, the tip dipole is given by  $\mu_t$  and the particle dipole is denoted as  $\mu_p$ . This geometry is described well by the theory of optical forces between two polarizable particles,<sup>23,24</sup> which predicts a time-integrated photoinduced force experienced by the sample particle as follows:

$$\langle \mathbf{F} \rangle \propto \left\langle \sum_i \text{Re}\{P_i^*(\mathbf{r}) \nabla E_i(\mathbf{r})\} \right\rangle \quad (1)$$

Here  $\mathbf{r}$  is the position of the particle dipole relative to the position of the tip dipole. The optically induced polarization experienced by the tip is indicated by  $P_i(\mathbf{r})$ , where  $i$  labels the  $\{x,y,z\}$  components of the polarization. The resulting force is thus dependent on the interaction of the polarization with the gradient of the optical electric field in the vicinity of the sample particle. The polarization is generally a complex quantity, and the force can be rewritten in terms of a gradient force  $F_g$  which arises because of field inhomogeneities, and a scattering force  $F_{sc}$ , which is related to the momentum transfer between the light fields and the polarizable objects:<sup>13,23</sup>

$$\langle \mathbf{F} \rangle = F_g + F_{sc} \quad (2)$$

Under the assumption that the spatial phase of the electric field in the junction is invariant on the length scale of the interaction, and the particles are small relative to the distance

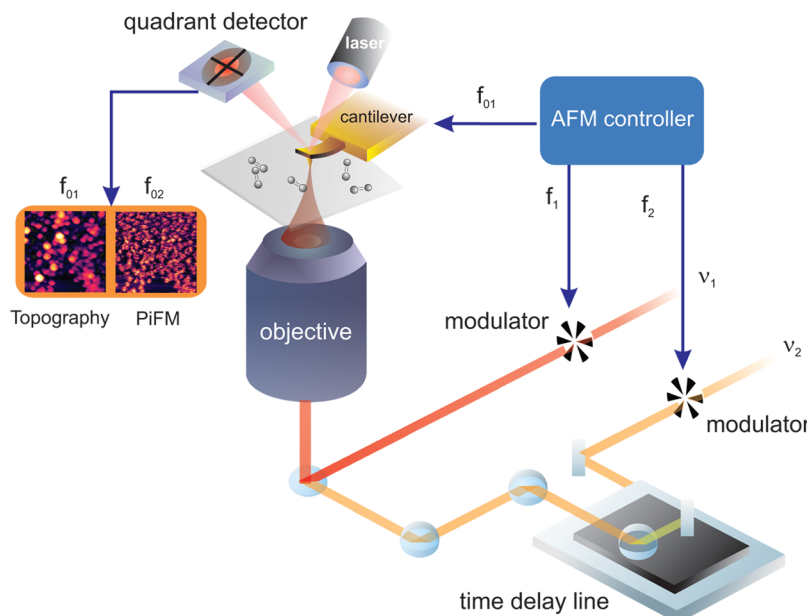


**Figure 2.** Basic layout of the photoinduced force microscope, shown here for a dual beam excitation configuration.

between the tip and sample, relatively simple expressions can be found for the gradient and scattering forces:<sup>22</sup>

$$F_g \propto \frac{1}{z^4} \alpha'_p \alpha'_t |E_{0z}|^2 \quad (3)$$

$$F_{sc} \propto \alpha''_t |E_{0x}|^2 \quad (4)$$

Here  $E_{0z}$  is the  $z$ -polarized component of the incident electric field, where  $z$  is directed along the longitudinal distance between the tip and sample. The  $x$ -polarized component of the incident field is denoted as  $E_{0x}$ . The polarizability of the tip and sample are written as  $\alpha_t$  and  $\alpha_s$ , respectively. The polarizability is a complex quantity, with real and imaginary components  $\alpha_{(t,p)} = \alpha'_{(t,p)} + i\alpha''_{(t,p)}$ . Under the assumptions made, it can be seen that the gradient force is sensitive to the spectroscopic properties of the sample particle, because it probes  $\alpha_p$ . The gradient force is furthermore sensitively dependent on the tip–sample distance, as it scales as  $z^{-4}$ , which leads to a highly localized force that is detectable only over tip–sample distances in the nanometer range. The scattering force in PiFM, on the other hand, is dominated by the dissipative part of the tip polarizability, and is thus less sensitive to the spectroscopic properties of the sample particle. In addition,  $F_{sc}$  displays a shallow distance dependence, defined by the spatial dimensions of the excitation field, and lacks the highly local nature of the gradient force. The challenge in PiFM is to sensitively probe the gradient force, which enables high-resolution spectroscopic imaging of the sample.

## THE PIFM INSTRUMENT

The PiFM instrument is an inverted optical microscope which utilizes an AFM detection head in place of a photodetector. Instead of detecting optical radiation, the primary signal in PiFM is the time-integrated, photoinduced force as registered by the AFM head. The light source in the PiFM system is a laser, which can be either a continuous wave (cw) or pulsed laser, depending on the type of optical experiment. For steady-state spectroscopic measurements, tunable cw laser light sources work well in PiFM. Ultrafast pulsed lasers can be

used for inducing forces that are a consequence of nonlinear optical excitations. Similar to all-optical pump–probe experiments, PiFM can be used to resolve the time-dependent excitation dynamics of chromophores, as will be discussed in a later Section. An impression of the layout of a nonlinear optical PiFM experiment is shown in Figure 2.

To discriminate the photoinduced forces from all other forces present in the tip–sample junction, the laser light beams are amplitude modulated. In the case of a dual beam, nonlinear optical excitation experiment, both beams are modulated at independent frequencies,  $f_1$  and  $f_2$ , respectively. Amplitude modulation can be carried out with acoustic-optic or electro-optic modulators. Typical modulation frequencies are in the 100 kHz to 10 MHz range, which allows data collection with short pixel dwell times and preserves the ability to acquire images at moderately high speeds. The light beams are subsequently coupled into the microscope frame and focused by a high numerical aperture (NA) objective. Focusing is needed to confine the illumination area, which minimizes light exposure of unexamined parts of the sample. In addition, since photoinduced forces are weak, focusing helps to increase the magnitude of the effect by raising light intensity in the illuminated spot. A typical objective used in PiFM studies is an oil immersion lens with a NA of 1.40.<sup>15,22</sup> Imaging is achieved by moving the sample relative to the position of the focal spot, commonly accomplished with a piezoelectric stage.

To detect the optical response of the excited chromophores in the sample, the tip of the AFM head is positioned in illumination spot. Precise positioning of the tip is critical, as the magnitude of the photoinduced forces is sensitively dependent on the spatial distribution of the focal fields. The gradient force is optimized through the presence of strong  $z$ -polarized fields, in line with the polarization direction in which the strongest surface fields at the atomically sharp tip are found.<sup>25</sup> For linearly polarized input fields, the  $z$ -polarized component of the field, which grows when focused with higher NA lenses, is found at off-axis positions in the focal spot.<sup>26</sup> Maximum gradient forces are thus measured when the tip is positioned off from the center of the focal spot, at the peak of the  $z$ -polarized

focal field.<sup>27</sup> Alternatively, radially polarized incident fields can be used,<sup>2,28</sup> in which case the maximum gradient forces are expected when the tip is placed on-axis in the focal spot.

The PiFM instrument is capable of simultaneously detecting the sample's topography and the photoinduced forces. The topography is registered in regular AFM mode using a cantilevered tip. The cantilever is actively driven at a mechanical resonance,  $f_{01}$ , with an amplitude  $A_1$ . This eigenfrequency may correspond to the first mechanical resonance of the cantilever, but in some cases, the second mechanical resonance can be chosen instead. The set point of the cantilever, which relates to the distance between the sample and the average cantilever position, is fixed and maintained through feedback control. The topography image is obtained by monitoring the amplitude and phase variations at the  $f_{01}$  resonance while the sample is moved relative to the (illuminated) tip. To detect the photoinduced force separately from other forces present in the tip–sample junction, it is detected at a mechanical frequency away from the  $f_{01}$  resonance of the cantilever. The cantilever–tip system exhibits multiple eigenfrequencies,<sup>29,30</sup> and detecting the effects of the optical modulation at an alternate eigenfrequency of the cantilever allows resonant detection of the otherwise weak photoinduced force. The alternate eigenfrequency is denoted as  $f_{02}$ , and may correspond to the second mechanical resonance of the cantilever, or any other, as long as it is different from  $f_{01}$ . For example, when  $f_{01}$  is chosen to correspond to the first mechanical resonance, the second mechanical resonance can be chosen as  $f_{02}$ .

The photoinduced force is detected by demodulating the registered motions of the cantilever at a frequency that contains information on the effective optical modulation frequency  $f_m$ . The modulation frequency is simply  $f_m = f_1$  when single beam excitation is used, or  $f_m = f_1 \pm f_2$  when dual beam excitation is used. Two main detection schemes can be recognized. In the first scheme, called direct-mode, the optical modulation is tuned into direct resonance with  $f_{02}$ , that is,  $f_m = f_{02}$ .<sup>22</sup> In the second scheme, the signal is demodulated at a sideband frequency of  $f_m$ . This scheme is called the sideband-mode, where the optical modulation is chosen such that the sideband frequency  $f_m \pm f_{01}$  is tuned into resonance with  $f_{02}$ .<sup>16</sup> Both schemes are sensitive to the photoinduced force, but they display different sensitivities to the sample's polarizability and the laser intensity. The sideband mode is more sensitive to the gradient force and displays a steeper dependence on the tip–sample distance, whereas the direct-mode is better suited for extracting quantitative information from PiFM measurements.

The locality of the measured gradient force is related to its confinement along the  $z$ -dimension. The  $z^{-4}$  dependence ensures that the gradient force is detectable for tip–sample distances of only a few nanometers, which also limits the lateral extent over which the force is manifest. This intrinsic local character of the gradient force stipulates that the spatial resolution of the PiFM method is not solely dictated by the spatial dimensions of the optical fields near the junction, which often exceed the 10 nm scale. The sharp tips used in PiFM are, therefore, not primarily optimized for confinement of the optical field, as they are in scattering-based near-field methods. Instead, tips are chosen based on their ability to register the local forces, similar to the conditions maintained for proper operation of AFM imaging. Field-enhancement through excitation of surface plasmon resonances at the tip increases the magnitude of the photoinduced force. Indeed, most PiFM

measurements are performed with tips coated with either gold or silver. However, PiFM measurements can also be carried out with nonmetallic tips, including bare Si tips,<sup>31</sup> indicating that field confinement alone is sufficient and that plasmonic enhancement is not necessarily required for successful PiFM experiments.

The PiFM measurements that follow in the remainder of this Account are obtained with a custom-designed inverted microscope outfitted with a sensitive AFM detection head (Molecular Vista Inc.) operating in amplitude modulation mode (AM-AFM) under ambient conditions. Unless otherwise noted, the laser light source used is a Ti:sapphire laser (Mai-Tai, Spectra-Physics) that provides ~200 fs pulses tuned to 809 nm with a repetition rate of 80 MHz. The secondary light source used in some of the experiments described herein is a synchronously pumped optical parametric oscillator (Insight OPO, Spectra-Physics), providing tunable fs pulses throughout the visible range. The beams are focused with a 1.40 NA oil immersion objective lens (Olympus). The silicon tips used in the experiments are coated with 30 nm gold, and mounted on a cantilever system (ACTGG, AppNano) with the following typical parameters for the first mechanical resonance:  $f_{01} = 300$  kHz, spring constant  $k_1 = 40$  N/m and a quality factor  $Q_1 = 500$ . The free oscillation amplitude is typically  $A_1 = 10$  nm. For PiFM, the properties of the second mechanical resonance are also important, they are as follows:  $f_{02} = 1.8$  MHz,  $k_2 = 1600$  N/m, and  $Q_2 = 800$ .

## ■ IMAGING PROPERTIES OF PIFM

### Photoinduced Forces in the Focal Volume

When linearly polarized input fields are used, the spatial variation of the photoinduced force (PiF) in the focal plane is expected to follow the shape of the  $z$ -component of the focal field.<sup>31</sup> Figure 3b shows an image that is obtained by focusing a linearly polarized laser beam to a tightly focal spot at a glass/air

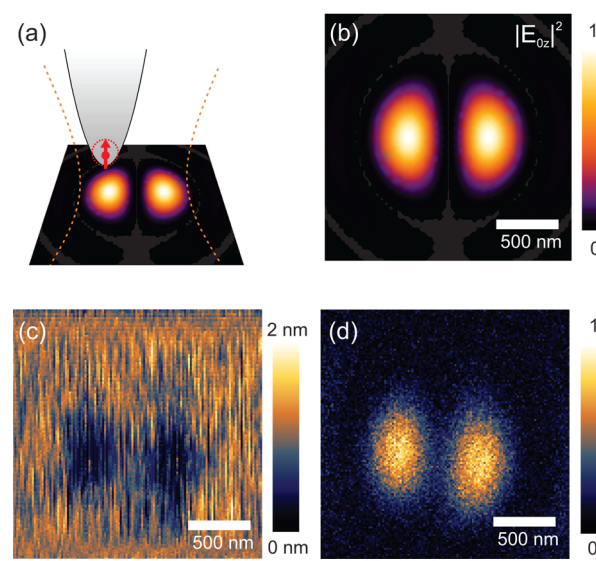


**Figure 3.** (a) Schematic of the tip in the vicinity of the focused optical field. The  $z$ -polarized part of the field interacts strongly with tip-dipole, which has its strongest component along  $z$ . (b) Simulation of  $E_z$ , the  $z$ -polarized component of the focused field by a high numerical aperture objective using linearly polarized input radiation. (c) Optical force artifact in the  $f_{01}$  detection channel when the tip is raster-scanned through the focused spot. (d) PiFM signal in the  $f_{02}$  detection channel.

interface, and mapping the magnitude of the PiF as the tip is scanned through the focal fields. It can be seen that the strongest photoinduced forces are indeed observed at the off-axis locations where the  $z$ -polarized field is maximized, shown in Figure 3c. This measurement also underlines that the PiFM approach can be used to precisely probe electric field distributions in the near-field, without relying on scattering radiation to a far-field photodetector.<sup>31</sup>

Whereas the image in Figure 3b is acquired by demodulating the signal at  $f_{02}$ , the topography image can be obtained simultaneously by demodulating the signal at  $f_{01}$ . For the glass/air interface examined here, no significant contrast is expected. Nonetheless, as shown in Figure 3a), the two-lobed pattern reminiscent of the  $z$ -polarized field distribution is also weakly observed in the  $f_{01}$  channel. This indicates that, besides the mechanical conservative forces that commonly govern the topographic contrast, a dc (nonmodulated) photoinduced force is detected as well. This effect has been previously noted in tip-illuminated AFM studies, and is known as the “optical force artifact”.<sup>32,33</sup> It results from the effective dc change in average tip–sample distance as a consequence of the sinusoidal modulation of the photoinduced force, which can be modeled as  $F_{\text{PiF}}(1+\cos(\omega_2 t))$ . At low average illumination powers of 100  $\mu\text{W}$  or less, this distance-dependent effect is usually sufficiently small as not to affect the topography image. However, for excitation powers over a mW, in combination with strong field enhancement at the tip, this effect is regularly observed in the  $f_{01}$  channel of PiFM measurements. Note that the artifact is only evident in the topography channel, and does not affect the contrast seen in the PiFM channel. Note also that the artifact discussed here is fundamentally different from other scan-probe artifacts such as topographic effects in s-SNOM measurements.<sup>34</sup>

#### Quantitative Analysis of PiFM Signals

In PiFM experiments of optically excited materials, the AFM head replaces photodetector for monitoring the optical response. However, the way in which a photodetector and the cantilever register the material’s optical response is fundamentally different. Whereas the electron current generated by a photodetector can be directly related to the number of photons emitted by the material, the relation between the material response and the motions of the cantilever are more complex. The main observables in the PiFM experiment are the amplitude  $A_2$  and phase of the cantilever oscillatory motions at the detection frequency  $f_{02}$ . The amplitude  $A_2$  is not a linear function of the magnitude of the light-matter interaction. An example is shown in Figure 4, where  $A_2$  is measured upon optical excitation of a nanocluster of silicon 2,3-naphthalocyanine (SiNC) dye molecules, while increasing the illumination power. It can be seen that at low illumination power,  $A_2$  scales roughly linear with laser power, whereas at higher powers  $A_2$  appears to level off and saturate. This plateauing effect results from the nonlinear dynamics of the cantilever itself and is unrelated to optical saturation of the sample. It is, therefore, imperative that the PiFM signal is properly modeled in order to retrieve the material response. The red line in Figure 4 shows that cantilever dynamics can be accurately described and understood, allowing retrieval of quantitative information from PiFM measurements.<sup>22</sup>

The amplitude  $A_2$  signal can be related to the magnitude of the photoinduced force, however, extracting such information requires a proper modeling of the cantilever dynamics.

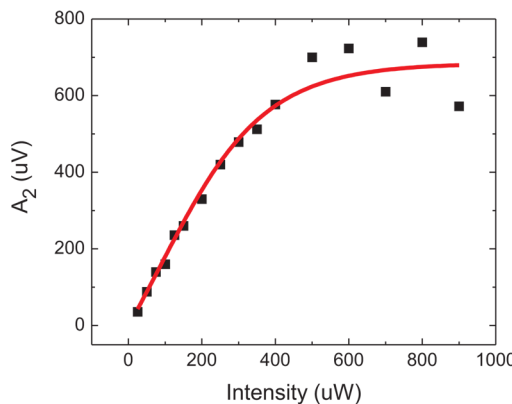


**Figure 4.** Amplitude of the cantilever resonance with respect to illumination power. The sample is a nanocluster of silicon 2,3-naphthalocyanine dye molecules on a mica substrate, and the laser excitation is set at 809 nm. The tip–sample set point is 10 nm. Experimental points are indicated by black squares and a simulation based on expected cantilever dynamics is shown as the solid red line.

Fortunately, such relations can be obtained for experimentally relevant conditions for the case of direct-mode detection. In the small oscillation limit,  $A_2$  can be related to the photoinduced force as<sup>22</sup>

$$|F_{\text{PiF}}(z)| = A_2(z) \sqrt{m^2(\omega'_2)^2 - \omega_2^2)^2 + b'_2 2\omega_2^2} \quad (5)$$

where  $\omega_2$  is the radial frequency of the cantilever resonance, and  $\omega'_2 = [(k_2 - (\partial \bar{F}_c / \partial z)|_z)/m]^{1/2}$  is frequency shift due to the presence of forces that act on the tip. In the latter expression,  $m$ ,  $k$ , and  $b$  are the mass, the spring constant, and a damping coefficient of a cantilever resonance, respectively.  $\bar{F}_c$  is a sum of the conservative force  $F_c$  of mechanical interaction and the dc  $F_{\text{PiF}}$ . Finally,  $b'_2 = b_2 + \Gamma(z)$ , where  $\Gamma(z)$  is a nonconservative force of mechanical interaction. The formalism expressed by eq 5 makes it possible to retrieve the photoinduced force, and thus the magnitude of the optical interaction through eq 3.

#### Linear Spectroscopy at the Nanoscale

One of the main advantages of PiFM over AFM is that the photoinduced force can contain spectroscopic information, allowing the generation of chemical maps at the nanoscale. According to eq 3, the gradient force is proportional to the real part of the optical polarizability. For optical transitions described by isolated, Lorentzian-like bands, the real part of the polarizability follows a dispersive line-shape. Hence, the spectroscopic signatures in PiFM are expected to be encoded in dispersive spectral features.<sup>21</sup> The red dots in Figure 5 depict the spectral variation of the PiFM signal recorded from a SiNC nanocluster. The real and imaginary optical response of SiNC are also shown in the Figure for the relevant range near 800 nm. It can be seen that the PiFM measurement traces the real part of the optical response. In principle, the absorption spectrum of the chromophore can be retrieved from PiFM experiments with the aid of a Kramers–Kronig transformation, although the original dispersive line shapes acquired in PiFM are often sufficient to spectroscopically resolve structures at the nanoscale. The dispersive line shape proves that the type of tip–sample interaction probed in PiFM is different than in thermal-expansion based nanoscopy techniques, which are based on the dissipative (imaginary) part of the material’s optical response. Note that in some circumstances, when the assumption of a slowly varying phase of the field is no longer

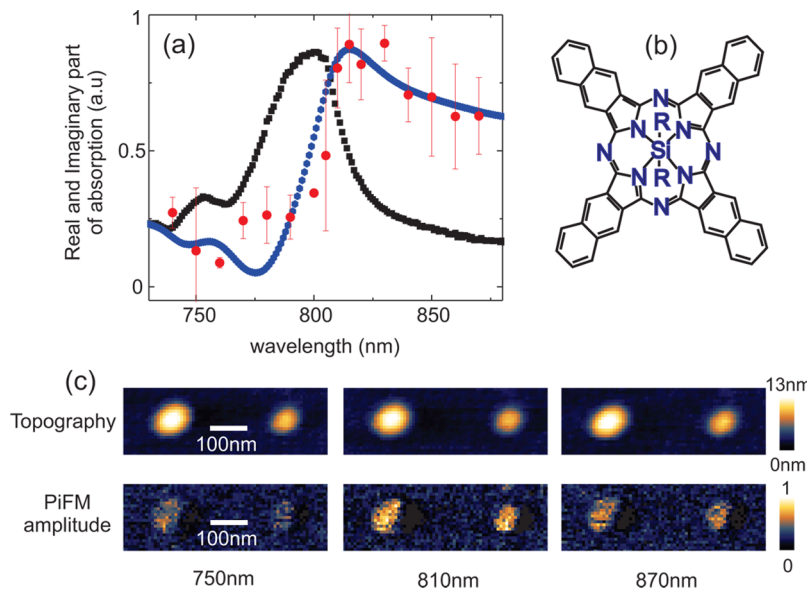


**Figure 5.** Spectroscopic sensitivity of PiFM. (a) Imaginary part (black dots) and real part (blue dots) of SiNc optical response. Red dots indicate the magnitude of the PiFM response. (b) Structural formula of SiNc. (c) Topography (top) and PiFM amplitude (bottom) of two SiNc nanoclusters as a function of excitation wavelength.

valid, PiFM signal may also contain contributions that are proportional to the imaginary part of the polarization.

#### PiFM Imaging Contrast

The image contrast in PiFM is determined by the optical polarizability  $\alpha$  of the material. However,  $\alpha$  is not the only parameter that controls the observed contrast in PiFM images. When operated in the direct detection mode, the PiFM experiment is sensitive to both the scattering and the gradient force. These two forces exhibit different dependencies on the tip–sample distance. While  $F_{sc}$  shows no marked variation on the nanometer scale,  $F_g$  changes dramatically due to its  $z^{-4}$  dependence. This implies that the contrast observed in the PiFM image can change significantly depending on the cantilever set point: for tip–sample distances of only a few nanometers, the gradient force dominates, while at larger distances the scattering force dominates. In addition, the  $F_g$  (attractive) and  $F_{sc}$  (repulsive) typically have opposite signs, implying that at a given distance, they may cancel each other. This is explained in Figure 6, which shows the force–distance

curve obtained from a SiNc nanocluster and from a bare glass substrate. It can be seen that, for short distances (pink region), the rapidly changing gradient force dominates, followed by a minimum where  $F_g$  and  $F_{sc}$  cancel each other, whereas at larger distances the shallow  $z$ -dependence of the scattering force is evident. The figure also shows that both the SiNc and the glass sample have similar force–distance curves, with the important exception that the SiNc sample gives rise to a stronger gradient force in the short-distance limit. The latter is a direct consequence of the much higher polarizability of SiNc, which was resonantly excited near 809 nm.

The blue range indicated in the figure, starting at zero tip–sample distance, represents the hard contact region. In this region, the cantilever shows static bending, making the system sensitive to thermal expansion of the sample. This is the limit most relevant to IR-AFM studies, which probe the absorptive properties of the specimen through the thermal expansion of the material.<sup>17–20</sup> PiFM, on the other hand, can be conducted in the noncontact to soft-contact (tapping) mode, measuring the electromagnetic forces in the junction rather than the expansion of the sample.

The characteristics of the force–distance curve are encoded in the PiFM images. In Figure 7, PiFM measurements are performed at two distinct cantilever set points. In Figure 7a and b, the topography and PiFM image of several SiNc nanoclusters are shown, respectively. These images are obtained for a large relatively tip–sample distance (18 nm). At this distance, the  $F_g$  contributions are expected to be negligible, and contrast is governed by  $F_{sc}$  and residual forces. As expected, under these conditions, no significant spectroscopic contrast is observed. The situation changes when the cantilever set point is changed to 8 nm, as shown in Figure 7c and d. Now the gradient force becomes prominent, and spectroscopic contrast, which was invisible at larger distances, can be observed in the PiFM image. Several nanoclusters seen in 7a are clearly resolved in the PiFM image.

It is also worthwhile pointing out that the topography image has changed upon lowering the cantilever set point. The

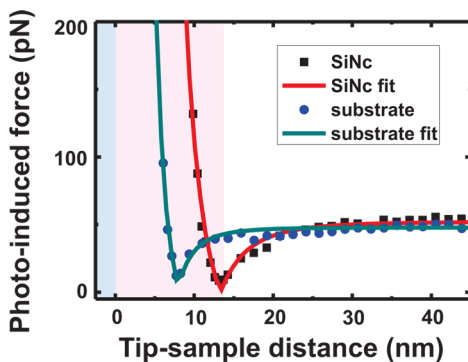


**Figure 6.** Photoinduced force distance curve measured on a SiNc nanocluster and on bare glass. Solid lines are simulations based on the formalism discussed in ref 22. The pink shaded region highlights the range in which the gradient force is dominant. The blue shaded region indicates the hard contact range.

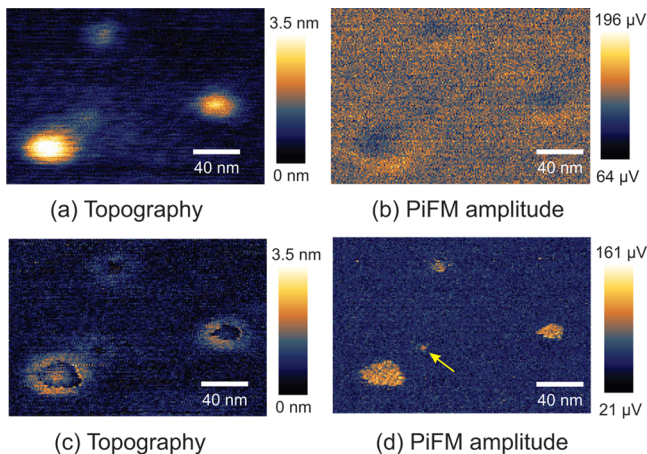


**Figure 7.** Contrast inversion with respect to tip–sample distance. (a) Topography and (b) PiFM image with 18 nm tip–sample distance, and (c) topography and (d) PiFM image with 8 nm tip–sample distance. Arrow points to a small feature of  $\sim 5$  nm diameter.

topography image now appears to carry a negative imprint of the PiFM image, resulting in indented structures. This is a manifestation of the “optical force artifact”, where the dc component of the photoinduced force is clearly resolved in the  $f_{01}$  channel. In this case, the optical force has an opposite sign relative to the effective mechanical interaction force experienced by the tip. It is interesting to note that the resolution of the PiFM signal is higher than that of the topography signal. This is a direct consequence of the steep  $z^{-4}$  dependence of the gradient force, producing a much more localized interaction than the long-range, van der Waals dominated mechanical interaction forces, which follow a shallower  $z^{-2}$  dependence.<sup>11</sup> The smallest feature in the Figure 7 measures  $\sim 5$  nm, which is clearly resolved in (d) but it is barely observed in the topography (a).

#### Nonlinear Optical Contrast in PiFM

PiFM measurements are not limited to linear optical excitations. Higher order optical effects, such as those described by the third-order polarization  $P^{(3)}$ , can also give rise to detectable forces. The nonlinear polarization of the particle can modify the polarization in the tip, and thus introduce a force component in the measurement that depends on nonlinear excitations in the sample.<sup>15,21,35</sup>

An example of a nonlinear PiFM experiment is shown in Figure 8. Here a SiNc nanocluster is illuminated with a femtosecond pulse pair. The first pulse at 809 nm, called pump, excites the SiNc molecule to the first excited state. A second pulse at 605 nm, called probe, subsequently excites the molecule to a higher lying excited state. To tune the experiment to this process of excited state absorption, the pulse trains are individually amplitude modulated at  $f_1$  and  $f_2$ , and the cantilever signal is demodulated at  $f_1 - f_2$ . In this fashion, only those photoinduced forces are measured that are brought about by both pulses. Upon delaying the probe pulse relative to the pump pulse, the photoinduced force decays exponentially, corresponding to the lifetime of the first excited state. The time-resolved PiFM experiment is thus sensitive to the same excited-state dynamics as probed in optical pump–probe experiments. The advantage of such a PiFM experiment is that force measurements can be performed on very small objects, down to the single molecule level, which is very

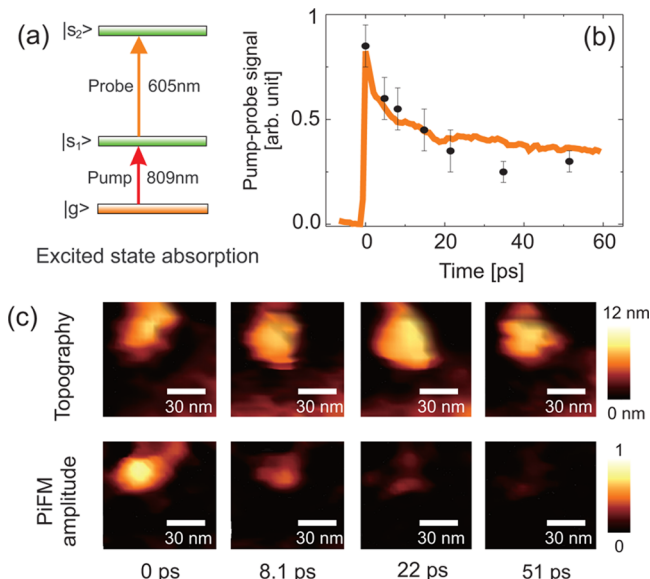


**Figure 8.** (a) Schematic of the pump–probe excitation of SiNc. (b) Time-resolved excited state absorption measured with PiFM (solid dots) and with optical pump–probe microscopy (solid line). (c) Topography (top) and PiFM signal amplitude (bottom) of a nanocluster measured at different time delay settings of the probe pulse.

challenging to accomplish with all-optical pump–probe experiments.<sup>15</sup>

Beyond electronic excitations, PiFM measurements can also be designed for probing vibrational excitations. For instance, using cw laser and a vibrational pump–probe scheme, stimulated Raman scattering signals from nanoclusters of selected chromophores have been measured.<sup>16</sup> Another example is given in Figure 9, where a stimulated Raman transition is triggered in coomassie blue with femtosecond pulses. The frequency of the excitation pulses is tuned such that their difference frequency  $\Omega$  matches the frequency of a strong ring vibrational mode near a Raman shift of  $1600\text{ cm}^{-1}$ . Figure 9b–d shows the topography of a nanocrystal of coomassie blue, measured for various settings of the frequency difference between the laser pulses. Whereas the topography is insensitive to  $\Omega$ , the PiFM signal displays a marked dependence on the frequency difference. Stronger signals are seen near  $1590\text{ cm}^{-1}$ , slightly red-shifted from the maximum of the Raman peak. These experiments demonstrate that PiFM allows measurements of nonlinear vibrational transitions on the nanoscopic scale, both with cw and femtosecond pulses.

#### ■ CHEMICAL IMAGING APPLICATIONS

The PiFM technique makes it possible to visualize nanoscopic materials with spectroscopic contrast. Good applications for PiFM are those in which a material exhibits (1) spatial variations on the nanoscale and (2) a detectable spectroscopic contrast. Naturally, materials with strong optical cross sections give rise to better contrast in the photoinduced force microscope. Examples include semiconducting nanoparticles, which display strong absorption features in the visible range of the spectrum and whose spatial dimensions are well matched with the resolution offered through PiFM. The photoinduced force microscope enables measurements on individual nanoparticles and can help characterize the linear and nonlinear optical properties of such materials.

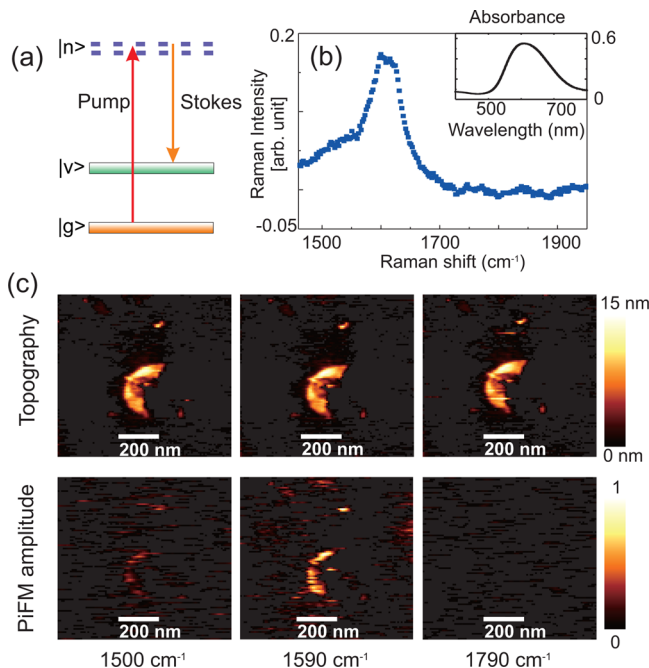


**Figure 9.** (a) Schematic of vibrational pump–probe excitation of Coomassie blue, corresponding to a stimulated Raman scattering process. (b) Raman spectrum and linear absorption spectrum (inset) of Coomassie blue. (c) Topography (top) and PiFM signal (bottom) of a Coomassie blue nanocluster measured for various difference frequency settings of the pump and probe.

Optical absorption measurements are not limited to the visible range of the spectrum. By changing the excitation wavelength to the mid-infrared range, PiFM contrast can be obtained from dipole-allowed excitations of vibrational modes. An example is given in Figure 10, which shows PiFM images of

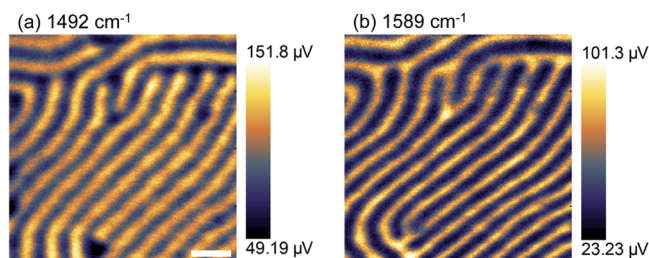


**Figure 10.** Chemical imaging of a thin film of a coblock polymer (PS-*b*-P2VP) based on IR-absorption contrast using a cw IR laser. (a) PiFM image taken at  $1492 \text{ cm}^{-1}$ . (b) Image taken at  $1589 \text{ cm}^{-1}$ . Scale bar is 100 nm.

a 30 nm thick film of a poly(styrene-*b*-2-vinylpyridine) coblock polymer. The expected pitch between the poly styrene (PS) and poly-2-vinylpyridine (P2VP) blocks is 46 nm, which is clearly revealed in the PiFM images. The  $1492 \text{ cm}^{-1}$  mode is stronger in PS, while the  $1589 \text{ cm}^{-1}$  mode is stronger in P2VP. Upon tuning the IR laser from  $1492$  to  $1589 \text{ cm}^{-1}$  mode, it can be seen that the contrast becomes inverted, illustrating the chemical imaging capabilities of PiFM.

Beyond nanoparticles and thin films, PiFM is also an excellent tool for probing the local surface fields of plasmonically active nano structures. Here the spectroscopic contrast originates from the spectral resonances of the surface plasmon fields. Using the sub-10 nm spatial resolution of PiFM, local

fields that govern such processes such as surface-enhanced Raman scattering (SERS) can be mapped out and studied in great detail.

## CONCLUSION AND OUTLOOK

PiFM enables spectroscopic probing with a resolution in the sub-10 nm range. Among the various scan probe techniques, PiFM stands out because of its high spatial resolution, achieved in the noncontact/tapping mode and at ambient conditions. Such conditions are ideal for the nondestructive visualization and characterization of a broad range of nanostructures materials. PiFM is a relatively new scan probe technique: the supporting theoretical modeling of PiFM signals is still in its infancy, and the ultimate limits of the technique have not yet been reached. There is no doubt that as PiFM matures as an imaging technology, the sensitivity and attainable resolution will continue to improve, qualities that will render the technique an important tool in the nanosciences.

## AUTHOR INFORMATION

### Corresponding Author

\*E-mail: [epotma@uci.edu](mailto:epotma@uci.edu).

### Notes

The authors declare no competing financial interest.

### Biographies

**Junghoon Jahng** is a Ph.D. candidate in the Department of Physics and Astronomy at the University of California, Irvine. His research is focused on the quantitative analysis of photoinduced force microscopy using both theoretical and experimental methods.

**Dmitry A. Fishman** is the Director of the Laser Spectroscopy Facility in the Department of Chemistry at the University of California, Irvine. His research is focused on nonlinear optical spectroscopy and microscopy, ultrafast phenomena and time-resolved spectroscopy of unequilibrated systems.

**Sung Park** is the CEO of Molecular Vista, Inc. (MVI), which develops instruments for tip-enhanced nanoscale optical imaging and spectroscopy. MVI has commercialized photoinduced force microscopy, which was invented at University of California, Irvine.

**Derek B. Nowak** is a staff scientist at MVI where he oversees the development of advanced near-field imaging microscopes. His primary research efforts involve pushing the limits of linear and nonlinear spectroscopic techniques to single molecule sensitivity.

**Will A. Morrison** is an applications engineer at MVI. He does experiments to improve and expand the functionality of MVI's near-field imaging microscope, the VistaScope, with a particular focus on refining and finding new applications for photoinduced force microscopy.

**H. Kumar Wickramasinghe** is the Henry Samueli Endowed Chair in Engineering at the University of California, Irvine. He has pioneered several scanning probe microscopes including the dynamic mode or noncontact Atomic Force Microscope. His current interest is in Bio Nanotechnology.

**Eric O. Potma** is an associate professor in the Department of Chemistry at the University of California, Irvine. His research group is active in developing nonlinear optical imaging techniques for the purpose of interrogating biological tissues, nanostructured materials and single molecules.

## ■ ACKNOWLEDGMENTS

The authors thank the National Science Foundation for financially supporting this work through Grant No. CHE-1414466.

## ■ REFERENCES

- (1) Hell, S. W. Far-field optical nanoscopy. *Science* **2007**, *316*, 1153–1158.
- (2) Anderson, N.; Bouhelier, A.; Novotny, L. Near-field photonics: tip-enhanced microscopy and spectroscopy on the nanoscale. *J. Opt. A: Pure Appl. Opt.* **2006**, *8*, S227–S233.
- (3) Stöckle, R. M.; Suh, Y. D.; Deckert, V.; Zenobi, R. Nanoscale chemical analysis by tip-enhanced Raman spectroscopy. *Chem. Phys. Lett.* **2000**, *318*, 131–136.
- (4) Pettinger, B.; Schambach, P.; Villagómez, C. J.; Scott, N. Tip-enhanced Raman spectroscopy: near-fields acting on a few molecules. *Annu. Rev. Phys. Chem.* **2012**, *63*, 379–399.
- (5) Schmid, T.; Opilik, L.; Blum, C.; Zenobi, R. Nanoscale chemical imaging using tip-enhanced Raman spectroscopy: a critical review. *Angew. Chem., Int. Ed.* **2013**, *52*, 5940–5954.
- (6) Pozzi, E. A.; Sonntag, M. D.; Jiang, N.; Klingsporn, J. M.; Hersam, M. C.; Van Duyne, R. P. Tip-enhanced Raman imaging: an emergent tool for probing biology at the nanoscale. *ACS Nano* **2013**, *7*, 885–888.
- (7) Knoll, B.; Keilmann, F. Scanning microscopy by mid-infrared near-field scattering. *Appl. Phys. A: Mater. Sci. Process.* **1998**, *66*, 477–481.
- (8) Huth, F.; Schnell, M.; Wittborn, J.; Ocelic, N.; Hillenbrand, R. Infrared-spectroscopic nano imaging with a thermal source. *Nat. Mater.* **2011**, *10*, 352–356.
- (9) Bechtel, H. A.; Muller, E. A.; Olmon, R. L.; Martin, M. C.; Raschke, M. B. Ultrabroadband infrared nanospectroscopic imaging. *Proc. Natl. Acad. Sci. U. S. A.* **2014**, *111*, 7191–7196.
- (10) Binnig, G.; Quate, C. F.; Gerber, C. Atomic force microscope. *Phys. Rev. Lett.* **1986**, *56*, 930–933.
- (11) Garcia, R.; Pérez, R. Dynamic atomic force microscopy methods. *Surf. Sci. Rep.* **2002**, *47*, 197–301.
- (12) Butt, H. J.; Cappella, B.; Kappl, M. Force measurements with the atomic force microscope: Technique, interpretation and applications. *Surf. Sci. Rep.* **2005**, *59*, 1–159.
- (13) Novotny, L.; Hecht, B. *Principles of Nano-Optics*; Cambridge University Press: Cambridge, UK, 2006.
- (14) Rajapaksa, I.; Uenal, K.; Wickramasinghe, H. K. Image force microscopy of molecular resonance: A microscope principle. *Appl. Phys. Lett.* **2010**, *97*, 073121.
- (15) Jahng, J.; Brocious, J.; Fishman, D. A.; Yampolsky, S.; Nowak, D.; Huang, F.; Apkarian, V. A.; Wickramasinghe, H. A.; Potma, E. O. Ultrafast pump-probe force microscopy with nanoscale resolution. *Appl. Phys. Lett.* **2015**, *106*, 083113.
- (16) Rajapaksa, I.; Uenal, K.; Wickramasinghe, H. K. Raman spectroscopy and microscopy based on mechanical force detection. *Appl. Phys. Lett.* **2011**, *99*, 161103.
- (17) Dazzi, A.; Prazeres, R.; Glotin, F.; Ortega, J. M. Subwavelength infrared spectromicroscopy using an AFM as a local absorption sensor. *Infrared Phys. Technol.* **2006**, *49*, 113–121.
- (18) Dazzi, A.; Prater, C. B.; Hu, Q.; Chase, D. B.; Rabolt, J. F.; Marcott, C. AFM-IR: Combining atomic force microscopy and infrared spectroscopy for nanoscale chemical characterization. *Appl. Spectrosc.* **2012**, *66*, 1365–1384.
- (19) Katzenmeyer, A. M.; Aksyuk, V.; Centrone, A. Nanoscale infrared spectroscopy: improving the spectral range of the photo thermal induced resonance technique. *Anal. Chem.* **2013**, *85*, 1972–1979.
- (20) Lu, F.; Jin, M.; Belkin, M. A. Tip-enhanced infrared nanospectroscopy via molecular expansion force detection. *Nat. Photonics* **2014**, *8*, 307–312.
- (21) Saurabh, P.; Mukamel, S. Atomic force detection of single-molecule nonlinear optical vibrational spectroscopy. *J. Chem. Phys.* **2014**, *140*, 161107.
- (22) Jahng, J.; Brocious, J.; Fishman, D. A.; Huang, F.; Li, X.; Tamma, V. A.; Wickramasinghe, H. K.; Potma, E. O. Gradient and scattering forces in photoinduced force microscopy. *Phys. Rev. B: Condens. Matter Mater. Phys.* **2014**, *90*, 155417.
- (23) Dholakia, K.; Zemánek, P. Colloquium: Gripped by light: Optical binding. *Rev. Mod. Phys.* **2010**, *82*, 1767–1791.
- (24) Arias-Gonzalez, J.; Nieto-Vesperinas, M. Optical forces on small particles: attractive and repulsive nature and plasmon-resonance conditions. *J. Opt. Soc. Am. A* **2003**, *20*, 1201–1209.
- (25) Roth, R. M.; Panouli, N. C.; Adams, M. M.; Osgood, R. M., Jr.; Neacsu, C. C.; Raschke, M. B. Resonant-plasmon field enhancement from asymmetrically illuminated conical metallic-probe tips. *Opt. Express* **2006**, *14*, 2921–2931.
- (26) Richards, B.; Wolf, E. Electromagnetic diffraction in optical systems II: Structure of the image field in an aplanatic system. *Proc. R. Soc. London, Ser. A* **1959**, *253*, 358–379.
- (27) Bouhelier, A.; Beversluis, M.; Hartschuh, A.; Novotny, L. Near-field second-harmonic generation induced by local field enhancement. *Phys. Rev. Lett.* **2003**, *90*, 013903.
- (28) Hayazawa, N.; Saito, Y.; Kawata, S. Detection and characterization of longitudinal field for tip-enhanced Raman spectroscopy. *Appl. Phys. Lett.* **2004**, *85*, 6239–6241.
- (29) Lozano, J. R.; Garcia, R. Theory of phase spectroscopy in bimodal atomic force microscopy. *Phys. Rev. B: Condens. Matter Mater. Phys.* **2009**, *79*, 014110.
- (30) Garcia, R.; Herruzo, E. T. The emergence of multifrequency force microscopy. *Nat. Nanotechnol.* **2012**, *7*, 217–226.
- (31) Huang, F.; Tamma, V. A.; Mardy, Z.; Burdett, J.; Wickramasinghe, H. K. Imaging nanoscale electromagnetic near-field distributions using optical forces. *Sci. Rep.* **2015**, *5*, 10610.
- (32) Kohlgraf-Owens, D. C.; Sukhov, S.; Dogariu, A. Optical-force-induced artifacts in scanning probe microscopy. *Opt. Lett.* **2011**, *36*, 4758–4760.
- (33) Kohlgraf-Owens, D. C.; Sukhov, S.; Greusard, L.; De Wilde, Y.; Dogariu, A. Optically induced forces in scanning probe microscopy. *Nanophotonics* **2014**, *3*, 105–116.
- (34) Ahn, J.; Chang, S.; Jhe, W. Incident polarization independence of topographic artifacts in scattering-type near-field microscopy. *Jpn. J. Appl. Phys.* **2008**, *47*, 4839–4842.
- (35) Kudo, T.; Ishihara, H. Resonance optical manipulation of nano-objects based on nonlinear optical response. *Phys. Chem. Chem. Phys.* **2013**, *15*, 14595–14610.